Coordinated Secondary Control for Balanced Discharge Rate of Energy Storage System in Islanded Microgrids

Guan, Yajuan; Guerrero, Josep M.; Quintero, Juan Carlos Vasquez

Published in:
Proceedings of the 2015 9th International Conference on Power Electronics and ECCE Asia (ICPE-ECCE Asia)

DOI (link to publication from Publisher):
10.1109/ICPE.2015.7167828

Publication date:
2015

Document Version
Early version, also known as pre-print

Coordinated Secondary Control for Balanced Discharge Rate of Energy Storage System in Islanded Microgrids

Yajuan Guan, Josep M. Guerrero, and Juan C. Vasquez
Microgrids research programme, Department of Energy Technology, Aalborg University, 9220 Aalborg, Denmark
Emails: {ygu, joz, juq}@et.aau.dk URL: www.microgrids.et.aat.dk

***Abstract*— A coordinated secondary control based on a novel autonomous currents sharing control strategy for balanced discharge rate of energy storage systems in islanded microgrid (MG) is proposed in this paper. The coordinated secondary controller is able to regulate the output power of distributed generating (DG) systems according to their state-of-charge by adjusting the virtual resistances of their voltage controlled inverters. This controller can not only provide the faster response and accurate output current sharing control, but also avoid the potential operation failure resulting from the over current and unintentional outage of DGs. Thus, the stability and reliability of islanded MG can be improved. The eigenvalues and root locus with the proposed controller are presented to design the parameters as well as analyzing the system stability. Simulation results based on Matlab/simulink are presented in order to verify the effectiveness of the proposed controller.**

***Index Terms*—Coordinated secondary control, energy storage system, balanced discharge rate, microgrid**

I. INTRODUCTION

NOWADAYS, the environmental issues, uncertainty of the prices for fossil fuels, concerns about the security of supply and the liberalization of the electricity markets result in a great change of the power system, the small scaled distributed generators is more promising comparing to traditional central power plant [1]. Microgrid (MG) has been proposed for several years as its capability of integrating different types of renewable energy sources [2].

Hierarchical control for MG has been proposed in order to standardize their operation and functionalities. The various functionalities such as voltage and frequency restoring, load sharing, resynchronization with the main grid, as well as the power flow exchanged between MG and the utility grid are classified and defined into three levels [3]. Moreover, more advanced and comprehensive functions for MGs can be achieved by combining the communication technology with the hierarchical control theory. A novel secondary control is proposed in [4] for improving the reactive power sharing performance among voltage controlled inverters (VCI) and restoring the frequency and amplitude deviations. A harmonic suppression control strategy based on secondary control for MG is proposed in [5]. A compensation control strategy based on secondary control scheme for unbalanced voltage of the point of common coupling (PCC) is represented in [6].

The MG defined by the Consortium for Electric Reliability Technology Solutions (CERTS) should able to supply the sensitive local load without the supporting of utility grid [7]. Therefore, the energy storage system (ESS) of MG should be charged either by the utility grid or the renewable energy sources in MG. Besides, the ESS should be discharged for peak shaving or supporting the local loads during the grid failure and electrical shortage to enhance the system stability and reliability [8]. However, there is a tradeoff between costs and the system reliability since the ESS is usually one of the most expensive components in practice [9]. A particle swarms optimization (PSO) based optimal capacity planning algorithm for ESS to reduce contract capacity of MG is proposed in [10].

Another issue is the sustainability of the islanded MG, which is dominantly decided by the balanced power exchange among distributed generation systems (DGs), ESSs and loads. Some previous works indicate that control capability of the ESS is limited by energy capacity of the storage device. If there are only the ESSs are involved in stabilizing and reliability of the MG, it may result in operation failure. Because the available electrical energy from ESS is affected by charging conditions, the ambient temperature, the charging and discharging current, as well as the ageing problem [11], [12]. The conventional power sharing control strategies mainly focus on the equal power sharing among different DG units. However, in fact, the ESSs in different DGs will have different discharge rate according to their state-of-charge (SoC). The powerless DG will be shut down when its SoC is below the threshold, while the rest of DGs have to supply more power for the local loads. This situation probably cause over current and outage, furthermore, degrading the stability and reliability of the MG due to the cask effect. To avoid this operation failure, the output power of the DG units should be coordinated in terms of their SoC. Some coordinated controllers are proposed for AC and DC MG [13]-[17]. For example, an ESS frequency bus-signaling of based autonomous active power control strategy is proposed in [13] for ac-islanded microgrids in order to achieve power management in a decentralized manner. However, these proposed controllers are all based on the droop control which has the relative slow transient response due to the low pass filter.

Therefore, a novel coordinated secondary control for balanced discharge rate of ESS in islanded MG is proposed in this paper. An autonomous current-sharing controller is employed in primary control to ensure the rapid and accurate loads sharing performance for the paralleled VCIs. The coordinated secondary controller is able to regulate the output power of DGs according to their SoC by adjusting the virtual resistances of the VCIs. This controller can not only provide the faster response and accurate output current sharing control, but also avoid the potential operation failure resulting from the over current and unintentional outage of DGs. Thus, the stability and reliability of islanded MG can be improved. The eigenvalues and root locus with the proposed controller are presented to design the parameters as well as analyzing the system stability. Simulation results based on Matlab/simulink are presented in order to verify the effectiveness of the proposed controller.

II. The Islanded Microgrid

A. The islanded microgrid

The configuration of an island MG is shown in Fig. 1. In daylight, the ESSs can operate in either charging or discharging mode according to the output power of PV panels and the consumption. The main function of ESS during the day is to balance the power between the renewable energy sources and local loads. While in the night, the ESSs will become the grid forming unit to maintain the common bus voltage and frequency, supply the local loads and fulfill the peak shaving functionality due to the lack of solar energy. In this situation, only the ESSs are involved in stabilizing and reliability of the islanded MG. In order to avoid the potential operation failure of MG and DGs discussed above, the output power of the DG units should be coordinated to share the load in terms of their SoC.

B. The characteristic of ESS

The valve-regulated lead acid (VRLA) battery is considered for ESS in this paper, since it can prove high number of charge-discharge cycles, low price, deep discharges and its practical use.

One of the most important issues of VRLA battery is the contradiction between the depth of discharge (DOD) and life-cycle as shown in Fig. 2. It can be seen that the DOD of VRLA battery decreases exponentially with the increasing of life-cycle. Therefore, SoC is usually limited to prevention of over discharge in practice. However, as the nonlinear characteristic and the unmeasurable of SoC, some complex models and advanced algorithms are developed for the accurate SoC prediction [18]-[19].

Another issue is the relationship of the rated capacity and the discharge current of VRLA battery as depicted in Fig. 3. It can be seen that the capacity of battery declines exponentially with the increasing of the discharge current. This phenomenon means that the total available electrical energy in VRLA battery may change according to the discharge condition even the batteries have the same initial SoC. Therefore, the ESS with smaller discharge current and balancing discharge rate may output more power compared to the equal power sharing control based system.

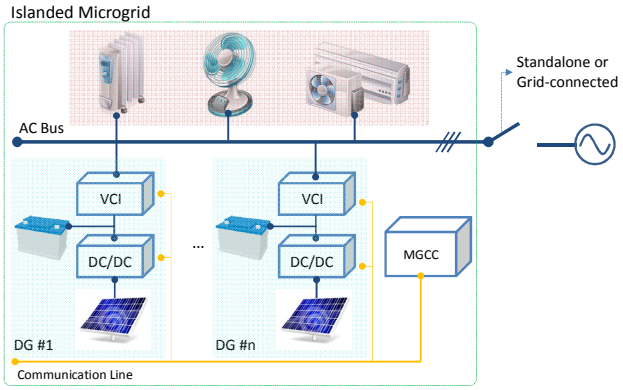

Fig. 1. The diagram of the islanded MG.

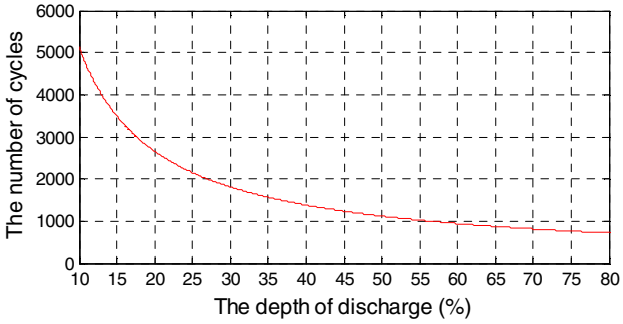

Fig. 2. The relationship between DOD and life cycles.

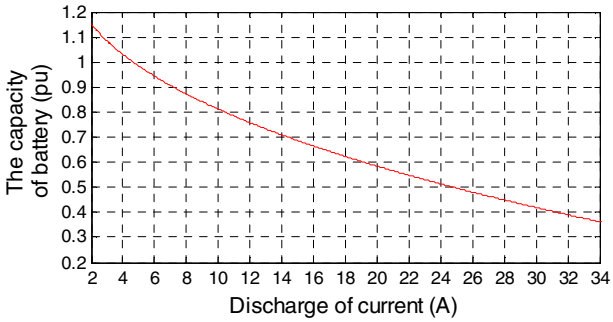

Fig. 3. The relationship between discharge current and the rated capacity.

C. The power sharing control of inverter

The autonomous current-sharing control strategy employed in primary control of this paper is depicted in Fig. 4. The controller consists of a virtual resistance loop (R_{vir}), a synchronous reference frame-based phase locked loop (SRF-PLL), a DC link voltage feed-forward loop, and the conventional P+R inner current and voltage loops (G_i and G_v) that generates a PWM signal to drive the IGBTs of the inverter. The current and voltage of inductor and capacitor are sampled and transformed to the stationary reference frame respectively.

The voltage reference v_o^* is generated by combining the amplitude reference ($|v_o^*|$) and the phase (θ) generated by a SRF-PLL. The SRF-PLL synchronizes all the inverters to the same frequency (ω^*). Even though

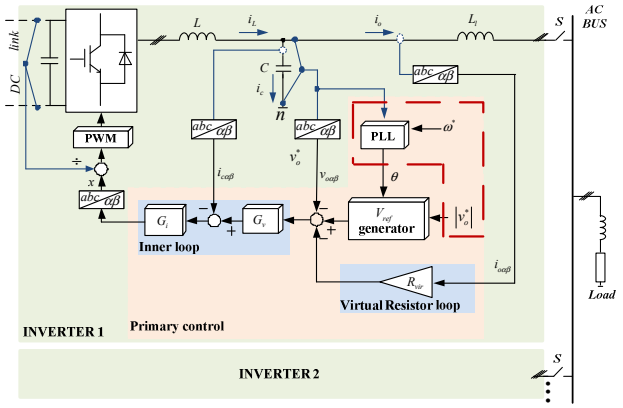

Fig. 4. The autonomous current-sharing control strategy.

the SRF-PLL is trying to synchronize the inverter with the common AC bus when supplying reactive loads, the current flowing through the virtual resistance will create unavoidable voltage drop that will cause the rising of frequency of the SRF-PLL. This inherent mechanism endows a droop characteristic in each inverter instead of adopting droop control loop. Therefore, the relationship between $I_{o\alpha}$, $I_{o\beta}$ and R_{vir} can be generalized and expressed for a number N of converters as:

$$I_{o\alpha 1}R_{vir1} = I_{o\alpha 2}R_{vir2} = \ldots = I_{o\alpha N}R_{virN}$$
$$I_{o\beta 1}R_{vir1} = I_{o\beta 2}R_{vir2} = \ldots = I_{o\beta N}R_{virN} \quad (1)$$

The output α and β axis currents of paralleled inverters are inversely proportional to their virtual resistances. It can be easily observed that current sharing performance is only influenced by the output impedance ratio instead of the output impedance value of these parallel inverters.

III. The Proposed Balanced Discharge Rate Control Strategy

As discussed above, the focus of the conventional power sharing control strategy in MG is to guarantee the equal power sharing among different DG units. Therefore, the identical virtual impedance R_{vir} is usually employed for all the DG units. However, the rated capacities and SoC values of ESSs in DGs are usually different. The discharge rate of DG_i (η_i) can be defined as following:

$$\eta_i = \frac{d}{dt}SoC_i = -\frac{k}{C_{bati}}P_{invi} \quad (2)$$

where $k = 1/3600$; C_{bati} is the rated capacity of ESS_i; P_{invi} is the output active power of DG_i. It can be seen that the discharge rate is influenced by the different rated capacities of ESSs and the output power of DG_i. Thus, the discharge rate (η_{equ}) can be adjusted to an identical value by regulating the virtual resistances (R_{viri}) based on their different SoC since the load current sharing ratio among DGs is dominated by the virtual resistances ratio. The control principle is shown in Fig. 5.

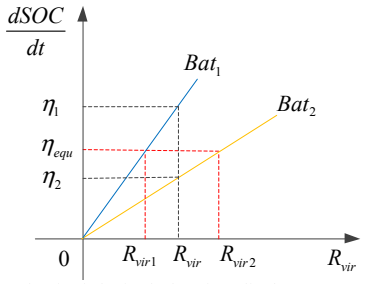

Fig. 5. The control principle for balancing discharge rate.

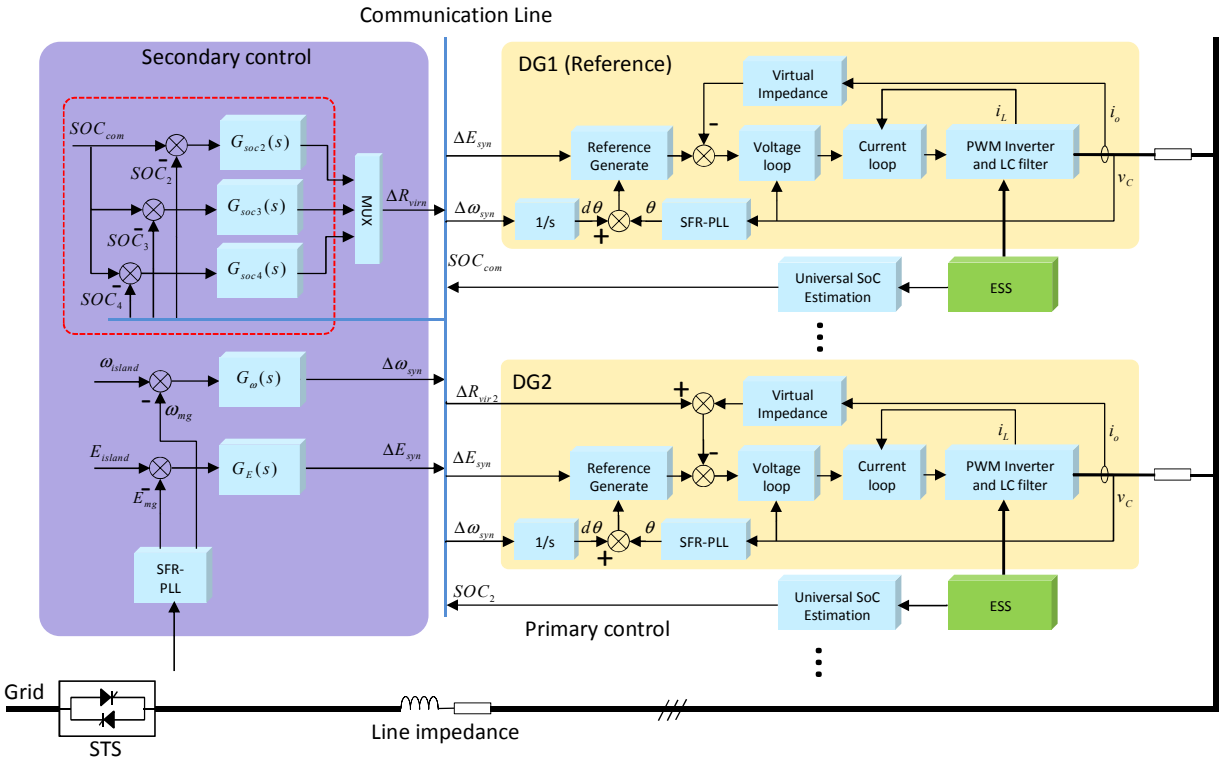

Fig. 6. The detailed control diagram of the proposed coordinated control strategy.

The detailed control scheme of the proposed coordinated secondary control strategy is shown in Fig. 6. The $\Delta\omega_{syn}$ and ΔE_{syn} are used for synchronization. A universal SoC estimation method is employed. The results of SoC estimation loop are fed back to secondary coordinated controller through communication line. Hypothetically, each ESS is fully charged at beginning, which means each initial SoC equals to 1. For balancing the discharge rate among DGs, an additional coordinating control loop is added in the secondary control level. Firstly, one of the DGs is selected as the common reference (SoC_{com}). Then the rest of DGs adjust their virtual resistances based on the differences between SoC_i and the common reference SoC_{com} by a PID controller expressed as follows:

$$\Delta R_{viri} = k_p(SoC_{com} - SoC_i) + k_i\int(SoC_{com} - SoC_i)dt + k_d\frac{d(SoC_{com} - SoC_i)}{dt} \quad (3)$$

where k_p , k_i and k_d are the parameters of PID controller. In order to depress the power oscillation among DGs, the output of the PID controller will be regarded as an incremental control part. Therefore, the virtual resistances of each DG can be presented as follows:

$$R_{viri} = R_{vir\_base} + \Delta R_{viri} \qquad i = 2,3,4.....N \quad (4)$$

IV. Small Signal Model and Stability Analysis

In order to analysis the system stability and parameters sensitivity, the small-signal model of the proposed coordinated secondary controller for balanced discharge rate has been developed in this section.

The consumption of the electrical energy of ESS_i can be represented by the integration of the output active power of DG_i (P_{invi}), as shown in Fig. 7. Therefore, the SoC of ESS_i can be calculated as follows:

$$SoC_i = 1 - \frac{k}{C_{bati}}\int P_{invi}\mathrm{d}t \quad (5)$$

where $k = 1/3600$; C_{bati} is the rated capacity of ESS_i.

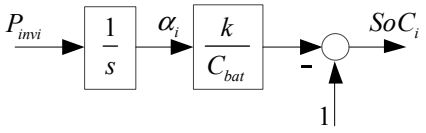

Fig. 7. The simplified model of the relationship between SoC and the output power.

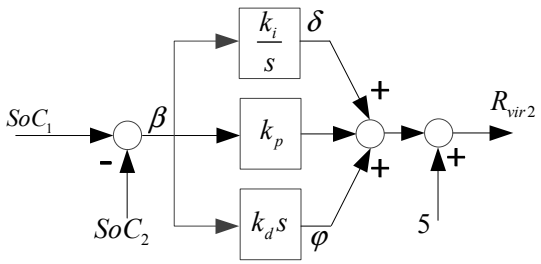

Fig. 8. Structure of the proposed coordinated secondary controller.

The small signal model can be derived as follows:

$$\Delta\hat{\alpha}_i = \Delta P_{invi} \quad (6)$$

The output equation of SoC_i can be written as follows:

$$SoC_i = \frac{\alpha_i k}{C_{bati}} \quad (7)$$

If there are two DGs in the MG, the coordinated secondary controller for balanced discharge rate can be shown in Fig. 8.

The small signal equation of variables β and δ are described in (8) according to Fig.8.

$$\begin{cases}\Delta\hat{\beta} = \frac{1}{k_d}\Delta\varphi = \frac{k}{C_{bat2}}\Delta P_2 - \frac{k}{C_{bat1}}\Delta P_1 \\ \Delta\hat{\delta} = k_i\Delta\beta = \frac{k_i k}{C_{bat2}}\Delta\alpha_2 - \frac{k_i k}{C_{bat1}}\Delta\alpha_1\end{cases} \quad (8)$$

Since the base value of virtual resistances of DG_1 and DG_2 are set to 5Ω, the relationship between ΔP_1 and ΔP_2 can be represented as follow:

$$\Delta P_1 = (\Delta P_2 + \frac{P_2\Delta\delta}{5} + \frac{\delta\Delta P_2}{5} + \frac{2k_d kP_2}{5C_{bat2}}\Delta P_2 - \frac{k_d kP_1}{5C_{bat1}}\Delta P_2 + \frac{k_p P_2\Delta\beta}{5} + \frac{k_p\beta\Delta P_2}{5}) / (1 + \frac{k_d k}{5C_{bat1}}P_2) \quad (9)$$

The complete state space model of MG can be derived as (10) by combining (6) ~ (9).

$$\Delta\hat{X} = A\Delta X + Bu \quad (10)$$

where $\Delta\hat{X} = [\Delta\alpha_1 \quad \Delta\alpha_2 \quad \Delta\beta \quad \Delta\delta]'$,

$$A = \begin{bmatrix} 0 & 0 & \frac{k_p P_2 C_{bat1}}{5C_{bat1} + k_d kP_2} & \frac{P_2 C_{bat1}}{5C_{bat1} + k_d kP_2} \\ 0 & 0 & 0 & 0 \\ 0 & 0 & \frac{-kk_p P_2}{5C_{bat1} + k_d kP_2} & \frac{-kP_2}{5C_{bat1} + k_d kP_2} \\ \frac{-k_i k}{C_{bat1}} & \frac{k_i k}{C_{bat2}} & 0 & 0 \end{bmatrix}$$

The system parameters are given in Table I.

Fig. 9 shows the trace of root locus when k_p increases from 100 to 1500 while k_d changes from 1 to 100. It can be seen that the dynamic response and oscillation damping performance of the system are improved as k_p increases from 100 to 1500. But finally, the dynamic response will decrease as the dominant modes move close toward the imaginary axis. As k_d increasing, the

TABLE I
THE PARAMETER OF SMALL SIGNAL MODEL

Parameter	Values	Parameter	Values
k_i	1000	C_{bat1}	100 Wh
k_p	500	C_{bat2}	200 Wh
k_d	10	P_2	1600 W
k	1/3600	P_1	800 W
R_{virdl}	5 Ω	R_{vird2}	5 Ω

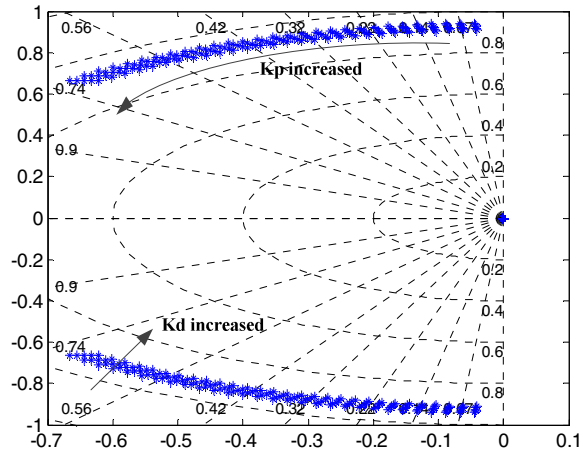

Fig. 9. Trace of nodes as function of $1 \le k_d \le 100$ and $100 \le k_p \le 1500$.

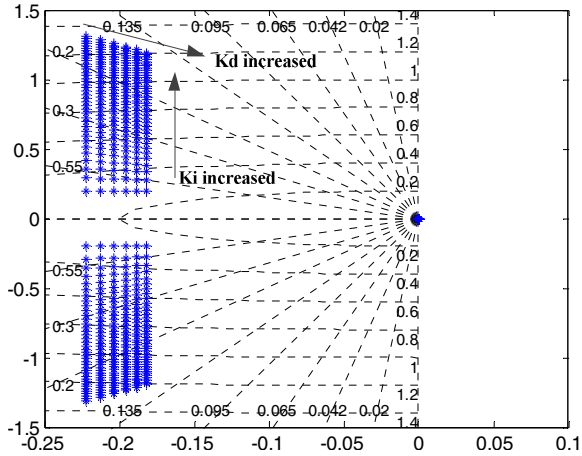

Fig. 10. Trace of nodes as function of $1 \le k_d \le 300$ and $100 \le k_i \le 2000$.

Fig. 10 shows trajectories of the modes in function of k_d increases from 1 to 300 while k_i increases from 100 to 2000. It can be seen that the complex poles trend to become the dominant modes, resulting in a near second order behavior. The imaginary parts of modes increase and move toward to the imaginary axis as k_d and k_i increasing, which will make the system become more oscillatory.

Fig. 11 shows the trajectories of the modes in function of k_i increases from 100 to 2000 while k_p increases from 100 to 1500. It can be seen that when the parameters increasing, the dominant modes move apart from imaginary axis which will improve the system dynamic response and oscillation damping performance.

V. Simulation and Verification

In order to compare and evaluate the performance of the proposed coordinated secondary control for balanced discharge rate, simulations based on MATLAB/Simulink are conducted. The simulation model is composed of three DGs with different ESS capacities, a constant load ($Load_{con}$), and a dynamic load ($Load_{dyn}$) for step up and step down test. The parameters of simulation models are listed in Table II. In this comparison, the control parameters for both conventional control and the proposed control are all the same.

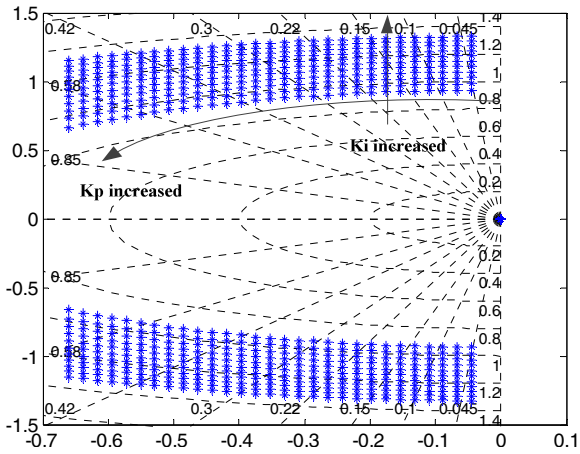

Fig. 11. Trace of nodes as function of $100 \le k_i \le 2000$ and $100 \le k_p \le 1500$.

TABLE II
The Parameter of Simulation Model

Parameter	Values	Parameter	Values
DG_1	4.5 kW	C_{bat2}	200 Wh
DG_2	4.5 kW	C_{bat3}	300 Wh
DG_3	4.5 kW	$Load_{con}$	5000 W
C_{bat1}	100 Wh	$Load_{dyn}$	3000 W

Before the comparison simulation, some assumptions need to be set. The first is the ESS_i for each DG is fully charged initially, thus all SoC_i are equal to 1. Then $Load_{con}$ sharing ratio among DGs is set to equal in conventional control simulation. $Load_{dyn}$ is connected and disconnected at 100s and 200s respectively. The threshold of SoC is assigned to 0.3 which means the DG_i has to be shut down to protect the ESS_i when SoC_i is below 0.3.

A. The simulation results with the traditional controller

The comparative simulation results with the conventional control strategy are shown in Fig. 12. It can be seen that output active power of each DG is controlled equally to share the loads with the traditional controller. Thus, the SoC of each DG decreases with different rates, since the rated capacities of ESSs are different.

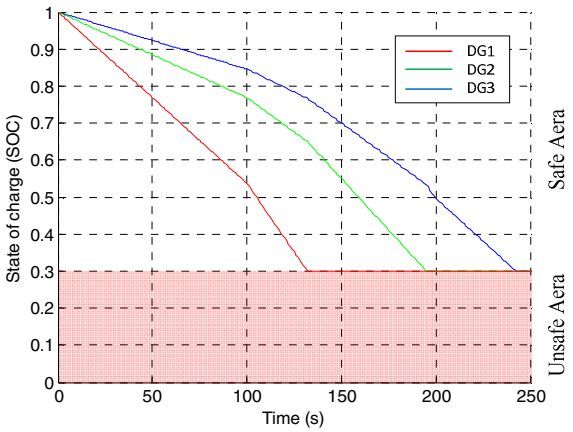

(a) The SOC of ESSs.

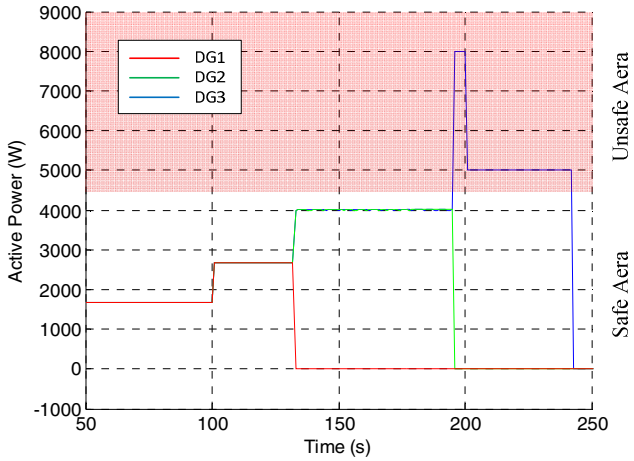

(b) The active power of DGs.

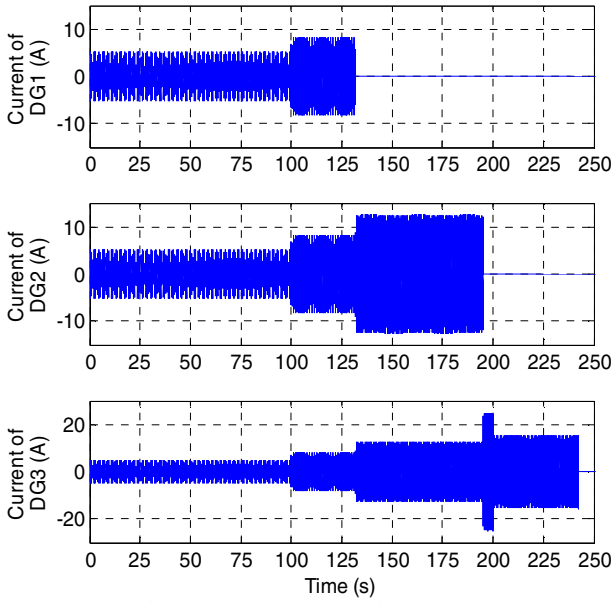

(b) The output currents of DGs (phase A).

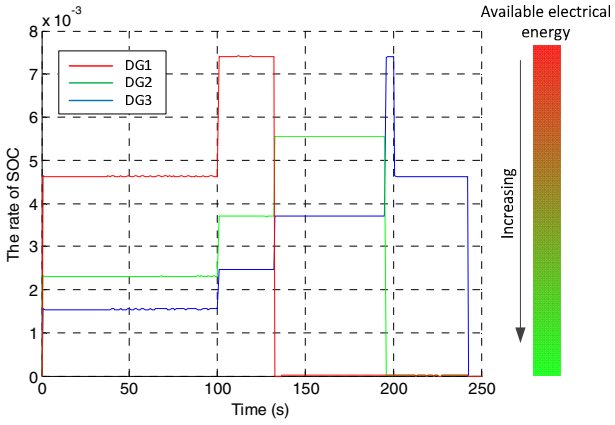

(d) The change rate of SOC.

Fig. 12. The simulation results with the conventional control strategy.

In this test, the DG_1 has the smallest ESS capacity. Therefore, the SoC of DG_1 decreases fastest with the unified output current. Then, the DG_1 is shut down at 131s when SoC_1 reaches 0.3, as shown in Fig. 12(a). Meanwhile, the output of DG_2 and DG_3 increase immediately to support the local loads as shown in Fig. 12 (b) and (c). At 193s, the DG_2 is shut down due to the SoC_2 is less than 0.3. The output power of DG_3 increases to 8kW which is far over its rated capacity since it has to take over all the local loads after 193s. Obviously, there is serious risk that will result in operation failure due to the over current in the real application. Therefore, the rated capacities of all the DGs have to be increased for allowance in order to avoid jeopardizing the reliability of MG. Moreover, in practice, the faster the DGs discharge, the less the electrical energy can be obtained totally as shown in Fig. 12 (d).

B. The simulation results with the proposed controller

The simulation results with the proposed control strategy are shown in Fig.13. The virtual resistances of DG_2 and DG_3 are regulated based on the outputs of the proposed coordinated secondary controller. In this way, these three SoC values decrease with the same gradient and reach the protection threshold simultaneously as shown in Fig. 13(a). It can be seen that the output active power and output current of DG units are different according to their SoC respectively, as shown in Fig. 13(b) and (c). Note that, there is no over current happens in Fig. 13(b). In other words, the operation failure can be effectively prevented. Thus, the redundant capacities of DGs and the costs can be reduced, and the reliability of MG can be increased. Furthermore, the discharge rate of ESS with the proposed controller in Fig. 13(d) is lower than the discharge rates in Fig. 12(d), which means more electrical energy can be obtain from ESS.

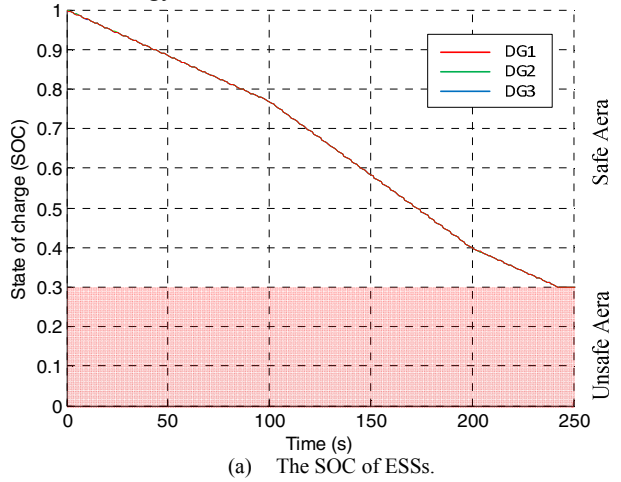

(a) The SOC of ESSs.

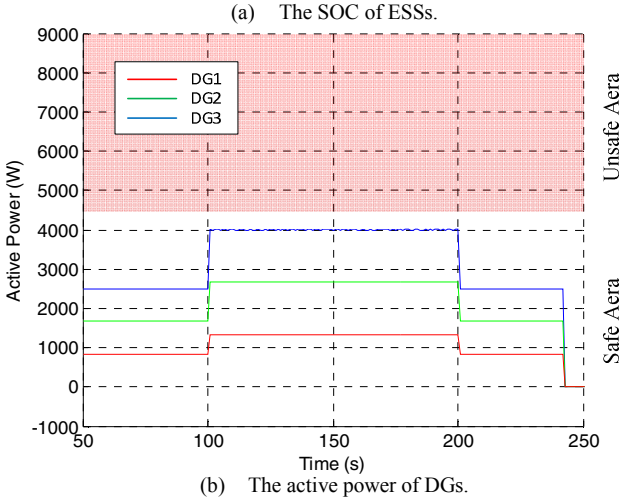

(b) The active power of DGs.

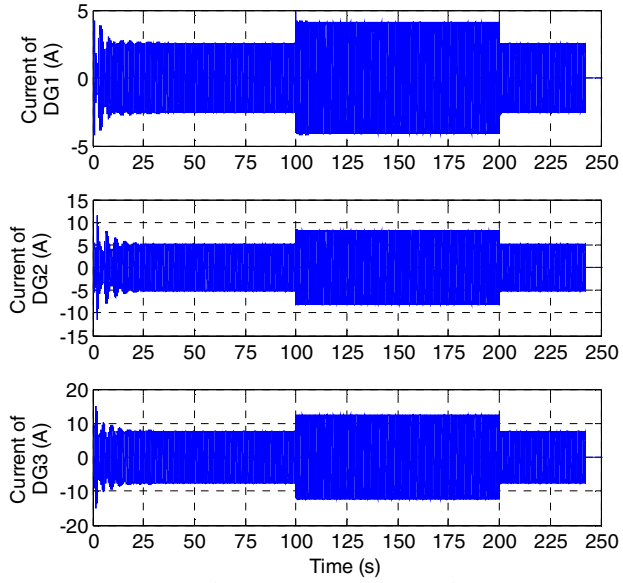

(c) The output current of DGs (Phase A).

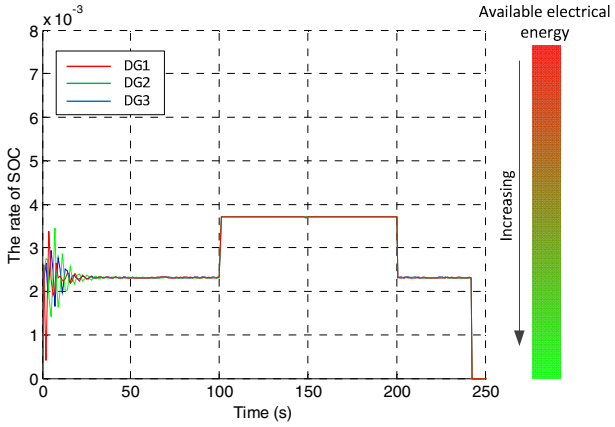

(d) The change rate of SOC

Fig. 13. The simulation results with the proposed coordinated secondary controller.

VI. CONCLUSIONS

A novel coordinated secondary control based on an autonomous currents sharing control strategy for balanced discharge rate of ESS in islanded MG is proposed in this paper. This controller can avoid the potential operation failure, provide the faster response and accurate output current sharing control, and improve the stability and reliability of islanded MG. The eigenvalues and root locus with the proposed controller are presented to design the parameters as well as analyzing the system stability. Simulation results based on Matlab/simulink verify the effectiveness of the proposed controller.

REFERENCES

[1] Blaabjerg, F., Zhe Chen, Kjaer, S.B, "Power electronics as efficient interface in dispersed power generation systems," IEEE Transactions on Power Electronics, vol.2, no.2, pp. 1184-1194, 2004

[2] Nikos Hatziargyriou, Hiroshi Asano, Reza Iravani, etc, "Microgrid," IEEE power & energy magazine, vol. 5, no.4, pp. 78-94, 2007

[3] Guerrero, J.M.; Chandorkar, M.; Lee, T.; Loh, P.C., "Advanced Control Architectures for Intelligent Microgrids-Part I: Decentralized and Hierarchical Control," IEEE Transactions on Industrial Electronics, vol. 60, no.4, pp. 1254 – 1262, 2013

[4] Q. Shafiee, J. M. Guerrero, J. C. Vasquez, "Distributed secondary control for islanded MicroGrids - A networked control systems approach," IEEE Transactions on Power Electronics, vol. 29,no.2, pp 5637 – 5642, 2014

[5] Savaghebi, M.; Jalilian, A.; Vasquez, J.C.; Guerrero, J.M., "Secondary Control for Voltage Quality Enhancement in Microgrids,", IEEE Transactions on Smart Grid, vol.3, no.4, pp.1893,1902, Dec. 2012.

[6] Savaghebi, M., Jalilian, A., Vasquez, J.C., "Secondary Control Scheme for Voltage Unbalance Compensation in an Islanded Droop-Controlled Microgrid," IEEE Transactions on Smart Grid, vol.3, no.2, pp. 797 – 807, 2012

[7] CERTS Microgrid Concept, http://certs.lbl.gov/certs-der-micro.html.

[8] de Almeida, A.T., Moura, P.S, "Minimization of energy storage requirements for a mixed renewable system with demand-side management," Industrial & Commercial Power Systems Technical Conference, Calgary, AB, 2009

[9] Ye Yang, Yang, N., Hui Li, "Cost-benefit study of dispersed battery storage to increase penetration of photovoltaic systems on distribution feeders" PES General Meeting Conference & Exposition, IEEE, National Harbor, MD, 2014

[10] Shu-Hung Liao, Jen-Hao Teng, Yung-Ching Huang, "Optimal Energy Storage System planning for microgrids with contract capacity constraint." ECCE-Asia, Hiroshima, 2014.

[11] A. G. Cannone, D. O. Feder, and R. V. Biagetti, "Lead-Acid Batteries: Positive Grid Design Principles," Bell System Technical Journal, vol.49, no.7, pp.1279 – 1303, 1970.

[12] Xiyu Liu, Wei Wang. VRLA, "Batteries System Reliability and Proactive Maintenance," Telecommunications Energy Conference (INTELEC), 32nd International, Orlando, USA, 2010

[13] Dan Wu; Fen Tang; Dragicevic, T.; Vasquez, J.C.; Guerrero, J.M., "Autonomous Active Power Control for Islanded AC Microgrids With Photovoltaic Generation and Energy Storage System," Energy Conversion, IEEE Transactions on , vol.29, no.4, pp.882,892, Dec. 2014

[14] Jong-Yul Kim; Seul-Ki Kim; Jin-Hong Jeon, "Coordinated state-ofcharge control strategy for microgrid during islanded operation," Power Electronics for Distributed Generation Systems (PEDG), 2012 3rd IEEE International Symposium on, pp.133-139, 25-28 June 2012

[15] Chendan Li, Dragicevic, T., Diaz, N.L., Vasquez, J.C., Guerrero, J.M., "Voltage scheduling droop control for State-of-Charge balance of distributed energy storage in DC microgrids," Energy Conference (ENERGYCON), 2014 IEEE International, 13-16 May 2014, Cavtat, pp: 1310-1314.

[16] Chendan Li, Garcia Plaza, M., Andrade, F., Vasquez, J.C., Guerrero, J.M., "Multiagent based distributed control for state-of-charge balance of distributed energy storage in DC microgrids," Industrial Electronics Society, IECON 2014, Oct. 29 2014-Nov. 1 2014, Dallas, pp: 2180 – 2184.

[17] Shafiee, Q., Dragicevic, T., Vasquez, J.C., Guerrero, J.M., "Hierarchical Control for Multiple DC-Microgrids Clusters," Energy Conversion, IEEE Transactions on, 2014, 29(4): 922-933.

[18] Gechen Li, Haiying Wang, Zhilong Yu. "New Method for Estimation Modeling of SOC of Batteries," Software Engineering, 2009, Xiamen, China.2009.

[19] Bhangu, B.S., Bentley, P., Stone, D.A., etc. "Nonlinear Observers for Predicting State-of-Charge and State-of-Health of Lead-Acid Batteries for Hybrid-Electric Vehicles," IEEE Transactions on Vehicular Technology. 2005, 54(3): 783-794.